Chem Catalysis

CellPress

Article

Accelerated analysis of the electrochemical production route for biomass-derived adiponitrile

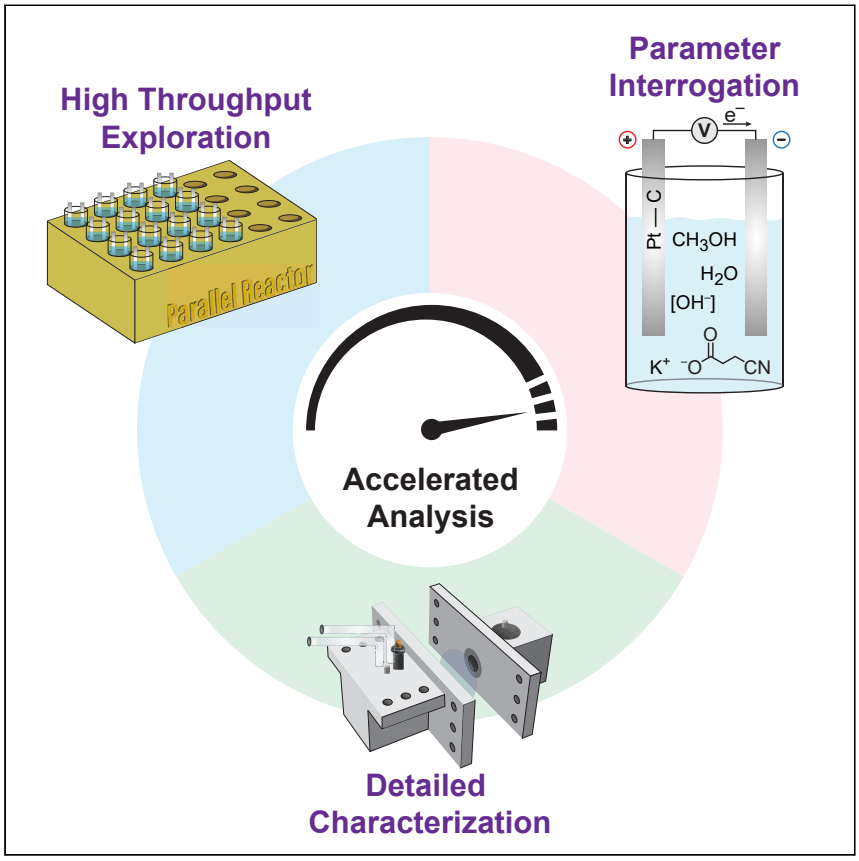

Adiponitrile is a key intermediate in the production of the essential polymer nylon 6,6. Here, we leverage high-throughput screening to establish relationships between key reaction parameters and product distributions in the electrosynthesis of adiponitrile from a biomass-derived substrate. We combine performance metrics with a high-level techno-economic analysis to give a perspective of the strategies that must be implemented to achieve scale-up of this process.

Ricardo Mathison, Elina Rani, Meera K. Patel, Antonio Lopez Cerrato, Casey K. Bloomquist, Miguel A. Modestino

modestino@nyu.edu

Highlights

Guidelines for the optimal electrosynthesis of adiponitrile via Kolbe electrolysis

Implemented a semi-autonomous high-throughput electrochemical workflow

Detailed analysis of the reaction to close carbon and electron balances

Presented techno-economic analysis to identify cost drivers and guide research

Mathison et al., Chem Catalysis 4, 100998
May 16, 2024
https://doi.org/10.1016/j.checat.2024.100998

Chem Catalysis

CellPress

Article

Accelerated analysis of the electrochemical production route for biomass-derived adiponitrile

Ricardo Mathison,[1] Elina Rani,[1] Meera K. Patel,[1] Antonio Lopez Cerrato,[1] Casey K. Bloomquist,[1] and Miguel A. Modestino[1,2,*]

SUMMARY

The electrochemical transformation of biomass feedstocks offers a promising route for the sustainable production of fuels and chemicals, enhancing integration with renewable energy sources. Adiponitrile, a key intermediate in nylon 6,6 production, is mainly produced through thermochemical processes or methods relying on fossil fuel feedstocks. Alternatively, it can be produced through the Kolbe coupling of biomass-derived 3-cyanopropanoic acid, with its practical implementation hinging on understanding and controlling factors that dictate reaction selectivity. In this study, we establish relationships between electrolyte composition, electrochemical conditions, and performance metrics in this approach, achieving a maximum faradic efficiency of 40% toward adiponitrile at current densities up to 500 mA cm^{-2}. Implementing a semi-autonomous high-throughput electrochemical workflow, we tested hundreds of reaction conditions, accelerating the exploration of reaction parameters. Limitations and guidelines obtained from this study apply to a range of electrochemical decarboxylation reactions, and the accelerated research approach shows potential for speeding up the development of sustainable electrochemical processes.

INTRODUCTION

Environmental, economic, and societal pressures are driving a transition from fossil resources toward renewable feedstocks for materials and energy production.[1,2] Biomass streams have the potential to serve as scalable feedstocks for the manufacture of sustainable fuels and carbon-based chemicals. However, these streams would need to be transformed through sustainable manufacturing processes into the required products to achieve substantial environmental benefits.

Electrocatalytic transformations of biomass feedstocks would enable chemical and fuel production under mild conditions (ambient temperature and pressure) and simplify the integration of renewable electricity into chemical processes.[1,3–5] For example, this approach could produce monomers and polymers from biomass feedstocks instead of fossil fuels, making plastic production more sustainable.[6] Recent demonstrations of electrocatalytic biomass transformations include monomer production from biomass refined sugar products (such as furfural),[7,8] aromatics production via electrochemical lignin conversion,[9,10] and paraffin, olefin, and alcohol production from the electro-oxidation of biomass-derived carboxylic acids.[11]

Nylon 6,6, used to produce high-performance textiles and structural materials, is one of the most important fossil-derived polymers manufactured by the chemical

THE BIGGER PICTURE

The chemical manufacturing industry's significant contribution to climate change is driven by its reliance on fossil fuels for feedstocks and energy. Electrocatalytic transformations of biomass-derived feedstocks circumvent both of these issues, leading to the integration of renewable energy sources and the valorization of sustainable carbon-based sources. Our study focuses on the electrosynthesis of high-value adiponitrile via Kolbe electrolysis of 3-cyanopropanoic acid, a derivative of glutamic acid. We used an accelerated electrochemical approach that involved high-throughput screening and detailed characterization to identify optimal conditions for this reaction. The mechanistic insights and limitations provided here are critical to guiding the deployment of this process at industrially relevant scales. In addition, the presented methodology of investigation could be used for a vast range of unexplored electrochemical reactions, helping to electrify and decarbonize the chemical industry.

industry. Thus, there is great interest in developing sustainable nylon production routes. Nylon 6,6 production relies on a key intermediate, adiponitrile (ADN).[12] The dominant approach for ADN production is the thermochemical hydrocyanation of 1,3 butadiene, which is an energy-intensive process that uses highly toxic reactants (e.g., hydrogen cyanide).[13–15] Alternatively, ADN can be produced electrochemically via the hydrodimerization of acrylonitrile (AN).[16–18] While this manufacturing route is one of the largest and most successful organic electrochemical processes practiced in industry, it relies on AN, a petrochemical feedstock, which limits the sustainability of ADN production.[1,19]

To eliminate petrochemical feedstocks and ultimately improve the sustainability of nylon production, ADN could be produced electrochemically using glutamic acid (GA) as a renewable feedstock. GA is the most abundant non-essential amino acid[20,21] and can be sustainably obtained from the hydrolysis of animal and vegetal waste proteins.[1,22] Previous studies have shown that GA can be converted through oxidative decarboxylation to 3-cyanopropanoic acid (CPA), which can then be converted to ADN via Kolbe electrolysis.[23] The first step—GA to CPA—can be achieved by several methods, including catalytic,[24,25] chemoenzymatic,[26] and electrochemical[23,27] conversion. The second step involves the Kolbe coupling of CPA, an electro-decarboxylation reaction that can upgrade carboxylic acids to high-value chemicals.

The electro-decarboxylation of carboxylic acids has been studied for over a century, since Hermann Kolbe first identified alkanes and CO_2 formation from acetic and valeric acid.[28] The reaction has multiple pathways with possible paraffin, olefin, and alcohol products, as extensively reported in the literature.[29–32] Scheme 1 presents the mechanism for the electrochemical synthesis of ADN through the Kolbe coupling of CPA. During the process, a carboxylate first undergoes an irreversible single electron transfer to the anode. Simultaneously, decarboxylation occurs, resulting in the generation of an alkyl radical and the release of CO_2.[3] These radicals can either dimerize to form ADN or disproportionate to produce AN and propionitrile (PN). Alternatively, the radical can be further oxidized to form a carbo-cation that when deprotonated forms the non-Kolbe product (AN). The carbo-cation can further react to form alcohols, esters, and other deep oxidation products. Parasitic solvent reactions can also occur at the anode surface, prominently the oxygen evolution reaction (OER) from water and methanol oxidation.

The product distribution in Kolbe electrolysis is heavily influenced by the electrode, electrolyte, and substrate structure. For Kolbe electrolysis to occur, the anode surface is assumed to be covered with alkoxy and alkyl radicals. Platinum (Pt) is the standard working electrode for Kolbe dimerization, which has a high resistance to electrochemical deactivation.[3] To promote non-Kolbe reactions, the most commonly used working electrode is graphite (C), which is more likely to degrade at higher anodic potentials.[3] A previous demonstration by Dai et al. identified several reaction conditions in which ADN can be produced through Kolbe coupling.[23] They showed that a mixture of methanol (MeOH) and acetone with KOH as an electrolyte led to the highest ADN yield in an undivided electrochemical cell. More recently, Kümper et al. demonstrated the synthesis of AN from GA in a two-step process with CPA as an intermediate.[27] The first step involved the electro-oxidative decarboxylation of GA and was achieved at yields of up to 97.6%. The second step focused on the non-Kolbe electrolysis of CPA at low current densities and with C as the working electrode. While these demonstrated a viable path for ADN electrosynthesis from biomass-derived feedstocks, an understanding of the key parameters that dictate

[1]Department of Chemical and Biomolecular Engineering, Tandon School of Engineering, New York University, 6 Metrotech Ct., Brooklyn, NY 11201, USA

[2]Lead contact

*Correspondence: modestino@nyu.edu

https://doi.org/10.1016/j.checat.2024.100998

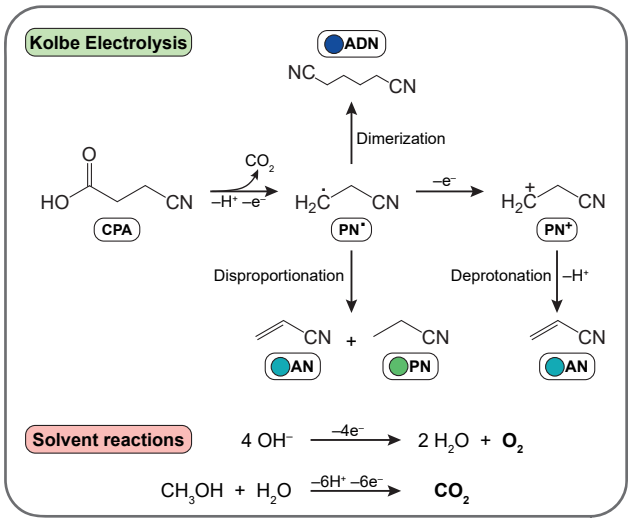

Scheme 1. Reaction mechanism for the Kolbe electrolysis of 3-cyanopropanoic acid
Proposed reaction mechanism for the formation of Kolbe products (ADN, adiponitrile; AN, acrylonitrile; PN, propionitrile), non-Kolbe product (AN, acrylonitrile), and solvent reactions (oxygen evolution reaction and methanol oxidation).

reaction selectivity and production rates and how to control those parameters to achieve high performance is required for practical implementation.

In this study, we used an accelerated electrochemical reaction engineering approach to establish relationships between electrolyte composition, electrode materials, electrochemical conditions. and product distribution in the Kolbe electrolysis of CPA to ADN and AN. Considering the reaction's extensive parameter space, achieving a thorough exploration via common research methods becomes infeasible due to the large number of experiments required. For this reason, we developed a hierarchical research approach that allowed us to simultaneously accelerate the exploration of a large number of reaction parameters as well as to study in detail the reaction under optimal conditions. The combination of results from this approach provided fundamental insights into the role of selectivity-controlling parameters. Furthermore, we performed a techno-economic analysis to understand the cost drivers and limitations and assess the viability of electrochemical ADN production using biomass feedstocks.

RESULTS AND DISCUSSION

Accelerated reaction characterization via an HTP hierarchical research approach

Given the large number of parameters that impact product distribution in Kolbe electrolysis, we developed a hierarchical electrochemical analysis approach to accelerate this study (Scheme 2). Establishing the interplay between key reaction parameters requires defining a parameter space for exploration. This is achieved by combinatorially selecting sets of parameters and performing electrochemical analysis under those conditions. For instance, three parameters with five different conditions each result in 125 unique reaction conditions. Facing this high number of experiments, a high-throughput (HTP) process becomes essential to obtain results promptly. Our approach consisted of a semi-autonomous, HTP electrochemical workflow that allowed us to collect large datasets and to train surrogate models that captured the complex relationships between reaction parameters and

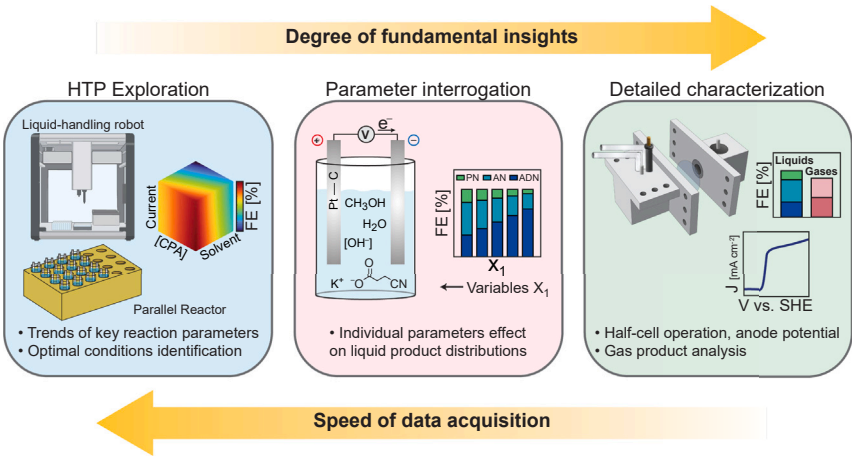

Scheme 2. High-throughput (HTP) hierarchical research approach for accelerated analysis of the electrosynthesis of adiponitrile from renewable feedstocks

performance. Leveraging this workflow, we then carried out a systematic investigation of the individual impacts of substrate concentration, alkali metal hydroxide, current density, pH, solvent composition, and electrode material on the selectivity of ADN production. To obtain deeper fundamental insight into this reaction, a different experimental technique with a slower throughput was required. For this reason, we only chose optimal conditions for Kolbe and non-Kolbe electrolysis to perform a detailed electrochemical characterization of the reaction, including complete product quantification in a gas-tight three-electrode cell. The hierarchical approach involved three sequential steps that together allowed us to rapidly elucidate complex relations between reaction parameters and performance:

Step 1: HTP exploration

Three key reaction parameters were selected for this study (current density, substrate, and solvent composition). We first designed a 3D parameter grid of >100 unique reaction conditions varying the three parameters. We then conducted experiments where these parameters were combinatorially varied using an HTP parallel electrochemical reactor[33] combined with a liquid-handling robot[34] for electrolyte preparation. This allowed us to achieve reaction exploration speeds of up to 20 reactions per hour. We used the collected data to train a Gaussian process regression (GPR) surrogate model that related the reaction parameters to the production rates and faradic efficiencies (FEs) of the products of interest (i.e., ADN or AN). While this step allowed us to substantially accelerate the exploration of reaction parameters, it had some key limitations: (1) it was not possible to collect gas products; (2) the operation in an undivided cell could result in the reduction of oxidation products; and (3) it was not possible to characterize the operating potential of the working electrode.

Step 2: Parameter interrogation

In this step, each reaction parameter was individually investigated to understand their impact on the CPA reaction pathways. Leveraging our HTP tools, we performed experiments in which each reaction parameter was varied while keeping all other parameters constant. Triplicate measurements were performed to ensure reproducibility. The results from this parameter interrogation step allowed us to derive relationships between the selected parameters and liquid product distributions and gain insights into key factors that drive performance. While this step provided a

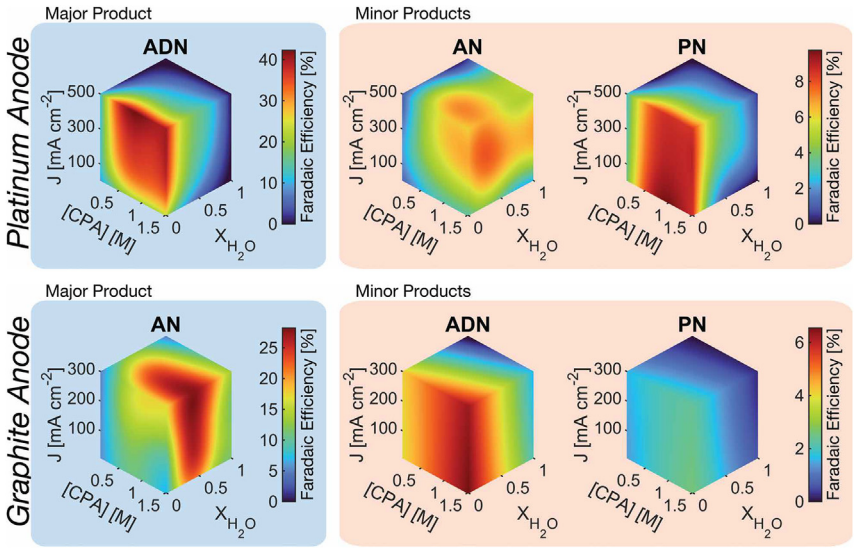

Figure 1. Mapping complex correlations between reaction parameters

Effect of current density (*J*), 3-cyanopropanoic acid (substrate) concentration, and electrolyte solvent composition (given by water solvent fraction, where methanol is the co-solvent) on the selectivity toward adiponitrile (ADN), acrylonitrile (AN), and propionitrile (PN) at a constant charge of 500 mA min, for platinum anode (top row) and graphite anode (bottom row). KOH was added to the electrolyte until a pH of 7 was reached. The results are derived from a Gaussian process regression model, trained on experimental observations dispersed through the entire 3D space: 157 data points for the platinum anode and 104 for graphite.

higher level of understanding, it still faced the same limitations of the HTP tools described in the previous step.

Step 3: Detailed characterization

To overcome the limitations of our HTP reactors, we designed and fabricated a gas-tight H-cell batch reactor and selected two sets of reaction conditions with maximum FE toward ADN (Kolbe product) or AN (non-Kolbe), respectively. With this custom reactor, we were able to (1) collect and quantify gas products, thus closing the electron balance, (2) separate the anodic and cathodic compartments with a membrane (i.e., Nafion), avoiding the parasitic reduction of anodic products, and (3) determine the anode potential, ensuring accurate and reproducible reaction conditions. This allowed us to achieve a detailed understanding of conditions that favored different reaction pathways in CPA electrolysis. It must be noted that experiments in this step had a substantially lower throughput (~1 experiment per hour) and required larger reaction volumes (~1.5 mL/reaction, vs. 0.6 mL/reaction for the HTP cells); thus, the broad exploration achieved in the previous steps would have been unfeasible.

Mapping complex correlations between reaction parameters

In the first step of our hierarchical approach, we performed an HTP reaction exploration to map the relationships between current density, substrate concentration, and solvent composition and FE toward ADN, AN, and PN. We conducted over 100 experiments using our HTP reactor using both Pt and C anodes, and the collected data points were used to train a GPR model (a non-parametric, probabilistic method).[35,36] The reactivity maps obtained from the GPR models are presented in Figure 1, detailing the FE toward each of the measured products. For all maps shown, the median standard deviation of the FE predictions was below 5%. Details

of how the presented surrogate models were built and information about their uncertainty can be found in Figures S1–S3.

The reactivity maps exhibit similar ADN and PN production trends for both electrodes. ADN and PN are predominantly produced at higher current densities and increased substrate concentrations, with pure MeOH as the solvent. This shared behavior suggests that both originate from the same PN radical (PN·) but follow two distinct reaction pathways: coupling or dimerization for ADN (the dominant pathway) and disproportionation for PN. In contrast, AN production can be produced through two pathways: the disproportionation of PN· or the deprotonation of a PN carbo-cation (PN^+). Consequently, we anticipated maximal AN production under conditions that promoted the oxidation of PN· and avoided their coupling to form ADN. Additionally, since AN can be hydrogenated at the cathode to form PN in the undivided HTP reactors, identifying conditions that hinder this parasitic reduction would enhance AN production. Our results show that AN production is optimized under conditions that involve higher current densities and substrate concentrations, likely due to the need to achieve significant electrode surface coverage of CPA and organic intermediates, which would effectively prevent solvent parasitic reactions. The highest AN selectivity was found in a solvent mixture of MeOH and water and using C electrodes, suggesting that modulating solvent solvation of intermediates (PN· and PN^+) with solvent mixtures and controlling parasitic solvent reactions is important to direct selectivity toward AN formation. Overall, we found that Pt electrodes operated at high current density and CPA concentration with low electrolyte water content lead to high ADN FE (up to 42%), while C electrodes at high CPA concentrations operated at high current densities with mixed water/MeOH solvents lead to high AN FE (up to 28%). These findings highlight how key parameters influence reaction pathways; however, analyzing each parameter individually is necessary to understand their specific effects on reaction performance.

Fundamental insights into selectivity-driving parameters

Effect of current density and metal anode

Pt is the most commonly used anode in Kolbe electrolysis due to its effective radical generation from carboxylic acids,[5] remarkable selectivity toward dimerized alkanes, and superior stability under anodic potentials, outperforming other electrode materials.[31,37,38] The prevalence of Pt in Kolbe electrolysis has motivated modeling studies on the reaction mechanism with these anodes, revealing that sluggish deprotonation of the acid on platinum oxide in aqueous conditions leads to high overpotentials for Kolbe products.[39] For non-Kolbe electrolysis, carbon materials are the preferred working electrodes.[5] However, graphite is prone to degradation at high anodic potentials, often requiring frequent replacement, highlighting the need for a more stable substitute for process longevity.[3] In our work, we used Pt and C electrodes because of their well-documented activity toward (non-)Kolbe electrolysis, allowing us to explore the effect of electrolyte composition and electrochemical conditions on CPA electrolysis.

Potentials exceeding 2.5 V vs. reversible hydrogen electrode are essential in Kolbe electrolysis for sufficient generation and coverage of alkoxy or alkyl radicals and to suppress water oxidation.[38,40,41] These elevated potentials need to be applied to reach high current densities which, when coupled with high carboxylic acid concentrations, enhance the yields of Kolbe products.[3] Unlike the Kolbe dimerization process, non-Kolbe electrolysis is favored by lower current densities, which favor the formation of carbenium ions.[37,42] Figure 2A presents the product distribution in CPA electrolysis using a Pt anode for current densities ranging from 35 to 480 mA cm^{-2}, under constant charge conditions and constant substrate concentration. The data illustrate an

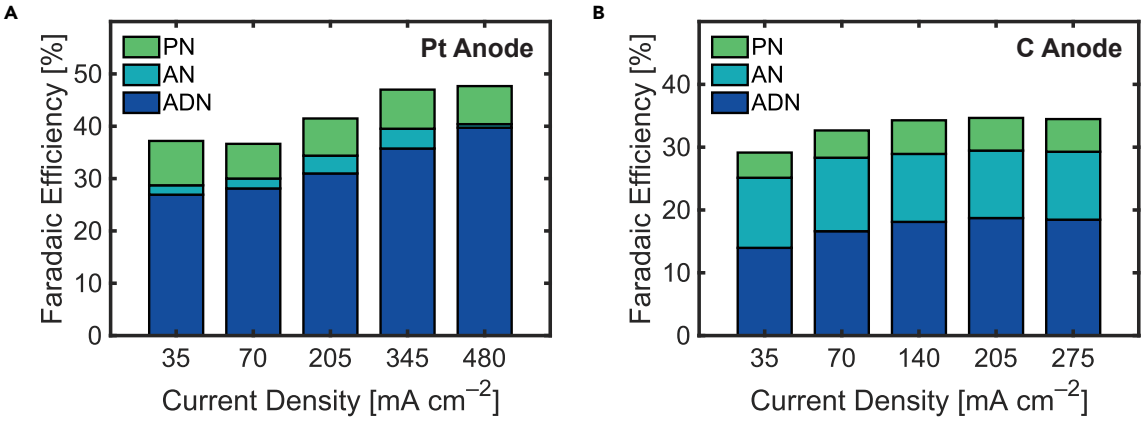

Figure 2. Effect of current density and metal anode

Effect of current density on selectivity toward adiponitrile (ADN), acrylonitrile (AN), and propionitrile (PN) at a constant charge of 500 mA min, platinum anode, and methanol solvent. KOH was added to the electrolyte until a pH of 7 was reached. The standard error on all the reported selectivity was <6%.
(A) Platinum (Pt) anode.
(B) Graphite (C) anode.

increasing selectivity toward ADN with greater current densities, consistent with previous studies on Kolbe electrolysis.[3] ADN FE plateaus toward 40% for current densities above 275 mA cm^{-2}. This behavior suggests that the dimerization rate becomes limited due to the saturation of alkyl radical coverage. Despite this observed limit in ADN selectivity, operating at the highest feasible current density would maximize ADN production rates. The production of AN and PN remains low under all explored conditions. Given the undivided nature of the HTP reactors, a fraction of the produced AN can be hydrogenated at the cathode to produce PN. This can explain the higher FEs observed toward PN.

The influence of the electrode material was investigated by exploring the impact of C on product distribution under the same conditions as the experiments performed with Pt electrodes. Selectivity values, as displayed in Figure 2B, were obtained for current densities ranging from 35 to 275 mA cm^{-2}. The current densities examined for C electrodes were kept below 300 mA cm^{-2} to mitigate the risk of the electrode degradation at the elevated anodic potentials. Consistent with observations from the Pt anode, the production of ADN was found to increase with current density. This can be attributed to the increased coverage of alkyl radicals on the electrode surface. Contrarily, when compared to Pt, C exhibited higher selectivity toward AN, which remained relatively constant with respect to current density. Echoing previous studies, these findings reaffirm the complex interplay between electrode material, current density, and product selectivity, thereby underscoring the need to carefully select of electrode materials and electrochemical conditions to optimize the formation of the desired products.

Effect of CPA concentration

The results detailed above underline the significant influence of the surface concentration of alkoxy or alkyl radicals on product distribution, highlighting the need for its control. This perspective is further validated by a recent study by Qiu et al., which conducted a comparative analysis of the reaction rates for the electrocatalytic decarboxylation reaction and OER.[43] The authors deduced that the product selectivities in both Kolbe and non-Kolbe electrolysis are contingent upon the surface coverage of intermediates derived from carboxylic acid and oxygen species. In addition, higher bulk

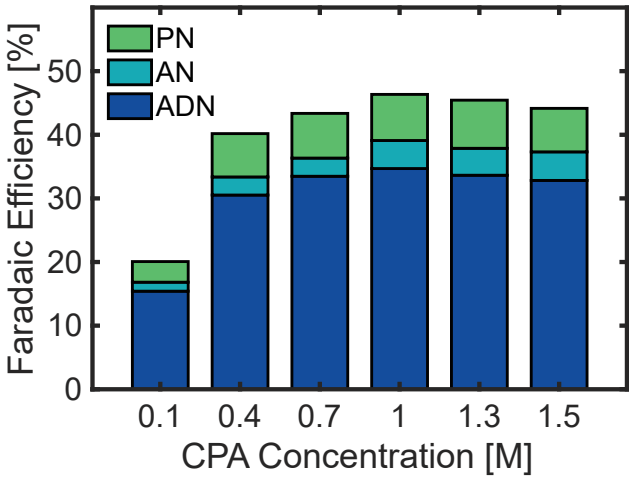

Figure 3. Effect of CPA concentration

Effect of 3-cyanopropanoic acid (substrate) concentration on selectivity toward adiponitrile (ADN), acrylonitrile (AN), and propionitrile (PN) at a current density of 140 mA cm^{-2}, platinum anode, and methanol solvent. KOH was added to the electrolyte until a pH of 7 was reached. The standard error on all the reported selectivity was <2%.

concentrations of carboxylic acids are associated with an increased electrode surface coverage, facilitating alkyl radical generation and enhancing Kolbe product selectivity.[38,44,45]

To elucidate the effect of substrate concentration on product selectivities, reactions were performed with varied CPA bulk concentrations ranging from 0.1 to 1.5 M—close to the solubility limit in MeOH—while keeping the rest of the reaction parameters constant. Figure 3 shows the selectivity toward liquid products for this concentration range. Larger CPA concentrations promote the formation of Kolbe products until it plateaus for concentrations >0.7 M. This suggests that maximizing electrode CPA coverage favors the formation of Kolbe products by effectively suppressing solvent reactions, thereby supporting the need for surface concentration control. Moreover, as Kolbe products require two equivalents of carboxylate, a large substrate concentration favors PN· coupling to form ADN.

Effect of alkali cation size

For an optimal Kolbe reaction, a neutral to weakly acidic environment is desired, typically achieved by neutralizing the carboxylic acid with an alkali metal hydroxide or alkoxide.[3] The size of alkali cations, considered to be electrochemically inactive species, profoundly impacts the reaction overpotential and product distribution. In the case of organic electrosynthesis reactions, molecular dynamics simulations have shown that larger cations (e.g., Cs^+) exhibit higher water coordination numbers with organic species and intermediate hydration strengths, thereby balancing water availability near the electrode region and controlling water side reactions.[46] Conversely, smaller cations (such as Na^+, with weaker hydration strengths) enhance the surface charge density and reduce reaction overpotentials due to a higher concentration in the electric double layer.[46] Similar results have been shown in the electrochemical reduction of CO_2, where the cation size has been linked to varying activity and product selectivity due to the electrostatic interplay between the solvated cations near the outer Helmholtz plane and the adsorbed species with large dipole moments.[47] These previous findings suggest that the size and concentration of supporting electrolyte alkali cations can control selectivity in electro-organic

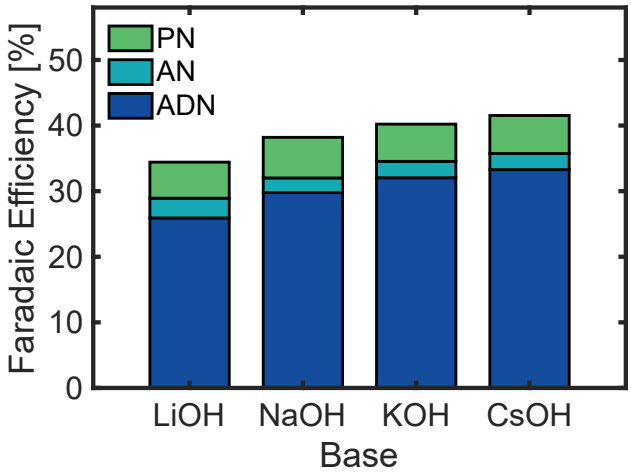

Figure 4. Effect of alkali cation size

Effect of alkali metal hydroxide on selectivity toward adiponitrile (ADN), acrylonitrile (AN), and propionitrile (PN) at a current density of 140 mA cm^{-2}, platinum anode, and methanol solvent. The base was added to the electrolyte until a pH of 7 was reached. The standard error on all the reported selectivity was <3%.

reactions through their solvation properties, and although these findings were based on reduction rather than oxidation reactions, alkali cation interactions with the carboxylate substrate and water in the diffuse layer are expected to have an effect on reaction kinetics and transport.

In our experiments we observe that larger cations favor selectivity toward organic products. Figure 4 presents the selectivity toward CPA-derived products as a function of alkali cation size. Given that a neutral pH was established prior to each reaction, the concentration of hydroxide remains constant across all cases, suggesting that the local concentration of the competing anion (OH^-) is unlikely to be a determining factor. It is worth noting that LiOH and NaOH have limited solubility in MeOH. Larger alkali cations appeared to favor the formation of ADN (i.e., ADN FE monotonically increases from 20% to 30% with increasing cation size), a finding that can be attributed to their capacity to constrain the availability of water molecules in the near-electrode region and to impact the electric field at the electrode/electrolyte interface.[47]

Effect of pH

The electrolyte pH can also strongly influence the product distribution, as it impacts the concentration of electrochemically active OH^- and H^+ ions as well as the protonation of the organic acid. For Kolbe electrolysis, the neutral or weakly acidic electrolytes are favored, as this ensures a nearly constant carboxylate concentration during electrolysis, even as the local anodic environment tends to shift to more basic pH values as a function of reaction time.[37] Previous studies have shown that weakly acidic electrolytes facilitate Kolbe product formation, while alkaline conditions that lead to higher deprotonation levels of the organic acid may also encourage the non-Kolbe pathway.[11,37,48,49] In our experiments the electrolyte pH was adjusted between 3.5 and 14 by adding various amounts of KOH to CPA solutions. Figure 5A presents the product selectivity across this pH range at a current density of 35 mA cm^{-2}. At acidic pH, the low concentration of deprotonated carboxylate results in low selectivity toward Kolbe reactions. In contrast, at basic pH, MeOH oxidation[50] and OER[51] become dominant, suppressing CPA oxidation reactions. Selectivity toward ADN was

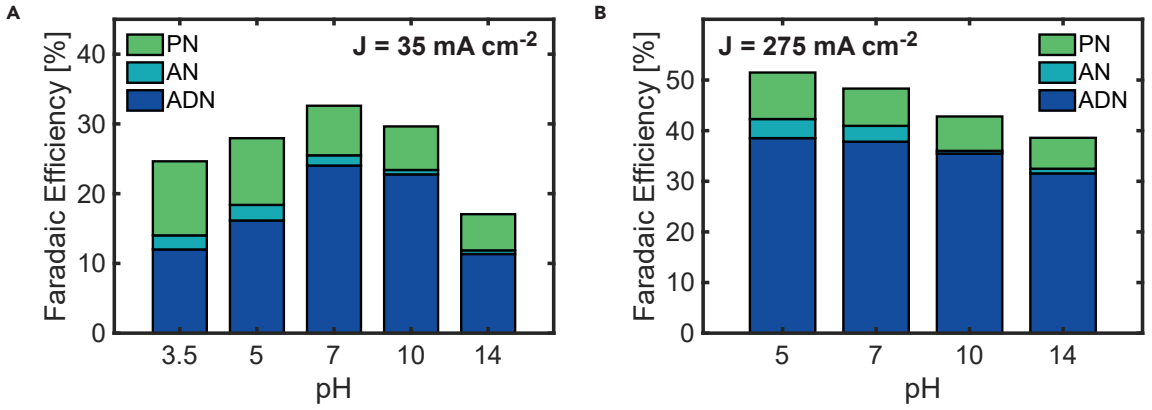

Figure 5. Effect of pH

Effect of electrolyte pH on selectivity toward adiponitrile (ADN), acrylonitrile (AN), and propionitrile (PN) using a platinum anode. Methanol was used as a solvent, and KOH was added to the electrolyte until the desired pH was reached. The standard error on all the reported selectivity was <2%.
(A) Current density of 35 mA cm^{-2}.
(B) Current density of 275 mA cm^{-2}.

maximized under neutral pH electrolytes. Further investigation of electrolyte pH was conducted at a higher current density of 275 mA cm^{-2}, as illustrated in Figure 5B. High current density electrolysis at a pH of 3.5 was limited due to the high electrolyte resistance, given that no KOH was added to the initial CPA solution to achieve this pH. The higher resistance required potentials beyond those achievable with our HTP experimental tools. Product selectivity between pH 5 and 7 remains relatively similar, likely due to the similar composition of the local electrode microenvironment given the low concentration of H^+ and OH^- ions. At higher pH values, selectivity toward organic oxidation products decreases, likely due to an increase in competing solvent reactions. While neutral to weakly acidic electrolytes enhance Kolbe electrolysis, these electrolytes are substantially more resistive, resulting in a higher energy requirement to maintain high current densities. High-concentration buffers can help mitigate these ohmic losses while at the same time maintaining a near-neutral pH that encourages the formation of Kolbe products.

Effect of solvent

Solvent selection directly impacts the reactant solubility, reaction efficiency, and product distribution in Kolbe electrolysis.[52] MeOH is widely considered to be the best solvent for this reaction because its oxidation is effectively inhibited by the formation a carboxylate layer at the electrode surface.[37] Other solvents, such as water and acetonitrile, can also be used for this reaction, but they tend to result in lower conversions and yields.[3] A recent study by Nilges et al. showed that water as a solvent leads to the formation of alcohols and esters from short carbon chain carboxylic acids through non-Kolbe electrolysis, while MeOH enhances selectivity toward the Kolbe product.[44] Figure 6A shows the product selectivity for CPA electrolysis in water/MeOH solvent mixtures. The results demonstrate that pure MeOH favors ADN production, and the production of this product decreases with the addition of water to the electrolyte. These results suggest that the increased water concentration enhances competing solvent oxidation reaction rates (i.e., OER), suppressing the oxidative decarboxylation of CPA. Furthermore, PN formation is significantly reduced in electrolytes with solvent compositions close to pure water, likely due to the suppression of the parasitic AN hydrogenation at the cathode as the competing hydrogen evolution reaction becomes more favorable.

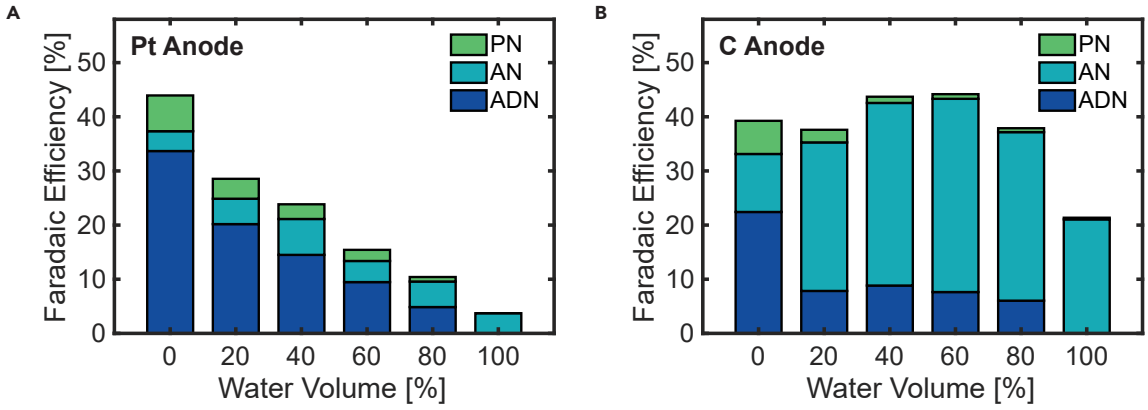

Figure 6. Effect of solvent

Effect of the electrolyte solvent composition on selectivity toward adiponitrile (ADN), acrylonitrile (AN), and propionitrile (PN) at a current density of 275 mA cm^{-2}, with methanol as the remaining solvent. KOH was added to the electrolyte until a pH of 7 was reached. The standard error on all the reported selectivity was <4%.

(A) Platinum (Pt) anode.

(B) Graphite (C) anode.

Results from Kolbe electrolysis with Pt electrodes showed that increasing water concentration in the electrolyte led to an increase of the non-Kolbe product, AN. To further investigate factors that promote AN formation, we performed experiments using C anodes, which are known to enhance the formation of non-Kolbe products. Figure 6B displays product selectivity for varying solvent compositions with C anodes. Similar to the observed behavior with Pt anodes, ADN production decreases with water concentration. In contrast, AN production is significantly promoted by the presence of water and is further enhanced by the use of C anodes, achieving a maximum FE of 35% for a solvent composition containing 40%–60% water. For MeOH-containing solvents, the total selectivity toward (non-)Kolbe products remains relatively constant, suggesting a similar electrode coverage of CPA-derived intermediates. The presence of water shifts the reaction pathway toward the oxidation of the PN· to PN^{+}, leading to the formation of non-Kolbe product (AN), suggesting that water solvation of the intermediate carbo-cation plays an important role in promoting the formation of AN.

Detailed reaction characterization under optimal conditions for ADN and AN production

The reactor and experimental approach described in the previous sections allowed us to rapidly study the relationships between key reaction parameters and the selectivity and production rates toward each of the organic liquid products. However, the HTP reactor did not have the capability to collect gaseous products or determine electrode potentials. Also, parasitic cathodic reactions could affect our assessment of the product distribution from CPA oxidation. One key observation that explains the relevance of parasitic cathodic reactions is that PN was produced at rates surpassing that of AN. If PN was only generated via the disproportionation of the anodically generated $PN^{\cdot}$ radicals, the production rates of AN and PN would be equal. Furthermore, since AN can also be produced by the deprotonation of PN^{+}, the expected anodic production rate of PN would necessarily need to be lower than AN production. This suggests that PN was in part produced from the cathodic hydrogenation of AN. Another significant finding was that the cumulative FE for all the liquid AN-derived products we analyzed peaked at ~50%, suggesting that a substantial fraction of the imposed current led to the generation of gaseous products not

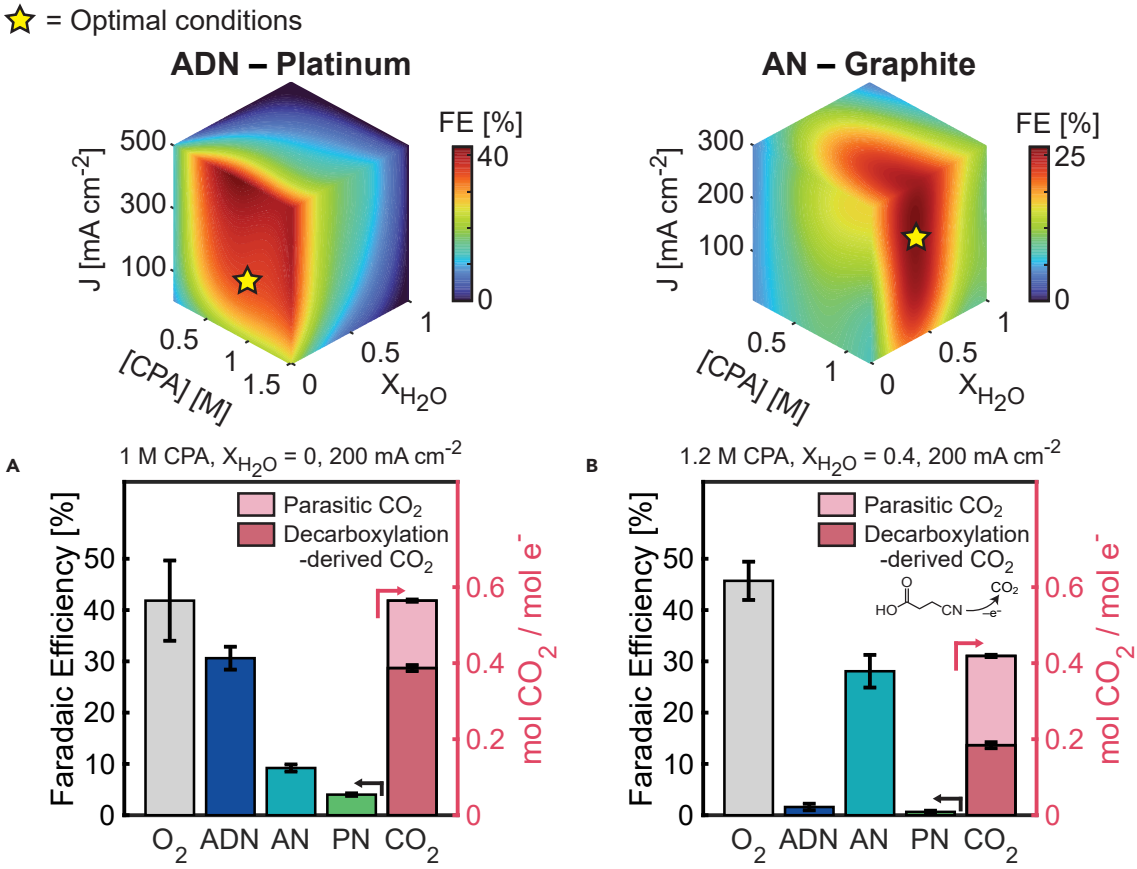

Figure 7. Detailed reaction characterization under optimal conditions for ADN and AN production

Product distribution of Kolbe and parasitic gas products on two selected operating conditions for adiponitrile (ADN) and acrylonitrile (AN) selective production. Selectivity toward O_2, ADN, AN, and propionitrile (PN) are represented by faradic efficiency (FE), and CO_2 production is shown as the ratio of moles of CO_2 produced and total moles of electrons passed during the electrolysis. The reaction conditions were chosen from the 3D mapping shown above as the optimal conditions for ADN and AN production. Reactions were carried at a constant charge of 500 mA min, and KOH was added to the electrolyte until a pH of 7 was reached. The results show (A) selective adiponitrile (ADN) production using a platinum anode and (B) selective acrylonitrile (AN) production using a graphite anode. Error bars represent the standard error on all the reported selectivity.

collected in our HTP reactor (i.e., oxygen from OER reaction or CO_2 from the oxidation of organic species).

To circumvent these characterization challenges, we designed a membrane-separated electrochemical reactor that allowed for divided cell operation as well as for gas collection. Further details on the design and operation of this reactor are presented in Figure S4. Based on findings from our HTP experimentation (step 1), two model conditions for the optimal production of ADN and AN, respectively, were chosen and characterized in detail in our membrane-separated reactor. The product distributions for both conditions are shown in Figure 7. The selectivity toward CO_2 is presented as the ratio of moles of CO_2 produced to moles of electrons transferred, since calculating the FE toward CO_2 is challenging due to multiple electrochemical pathways that could lead to its production (e.g., CPA decarboxylation, MeOH oxidation, graphite decomposition, and overoxidation of organic species). The calculations did not include dissolved CO_2.

Under both reaction conditions, oxygen is the dominant by-product, with an FE above 40%, surpassing the ADN maximum FE of 31% and AN maximum FE of 28% in their

respective optimal production conditions. In the reaction performed with Pt anode, there was significantly larger FE toward AN than PN, whereas the opposite was found in the undivided reactor, demonstrating that AN hydrogenation can be effectively prevented by using a membrane to separate the anolyte from the catholyte. Analyzing the expected CO_2 production from CPA decarboxylation provides additional insights into the selectivity of Pt and C anodes toward (non-)Kolbe electrolysis. Under the studied conditions, Pt was twice as selective as C for CPA decarboxylation, whereas C showed a higher rate for parasitic CO_2 production, likely due to oxidation of MeOH and the electrode itself. Although Pt is more selective for CPA decarboxylation, the potential required to operate at this optimal condition is exceptionally high (11.5 V vs. standard hydrogen electrode [SHE], see Figures S5 and S6). iR-compensated linear sweep voltammetry curves for both studied electrodes (see Figure S7) show that potentials required to operate at high current densities (>100 mA cm^{-2}) under MeOH-containing electrolytes are in excess of 5 V vs. SHE. Our findings underscore the need to develop more selective and energy-efficient Kolbe electrocatalysts that suppress the OER and to develop strategies to mitigate CPA transport limitations at high current densities.

Assessing the economic viability of GA-derived ADN

An economic assessment of biomass-derived ADN production is required to guide future research strategies, which can be extended to other Kolbe electrolysis reactions. Having identified optimal operation parameters for ADN production from CPA, we performed a high-level techno-economic analysis (TEA) of the viability of this bio-based production pathway to identify key technical and cost drivers that dictate its economic competitiveness (excluding separation and purification costs). Results from this TEA were aimed at shaping the direction of future research and development strategies for a feasible production of sustainable ADN. We estimated the levelized cost of ADN production (LCAP) as[53]

$$\mathrm{LCAP} = \frac{\sum_{t=1}^{t=n} \frac{I_t}{(1+r)^t}}{\sum_{t=1}^{t=n} \frac{P}{(1+r)^t}}, \qquad \text{(Equation 1)}$$

where P represents the annual production rate of ADN and I_t denotes the estimated annual investment in year t to maintain this level of production. I_t depends on electricity costs, capital expenses (cost of the electrolyzer), and the price of CPA, the primary raw material. Data sources for electricity[54] and capital expenses[55] were extracted from publicly accessible reports. CPA cost was estimated based on the price of GA[56] and the estimated cost for its oxidative decarboxylation to CPA.[57] For the LCAP calculation, we considered a range of costs for each component, noting that extreme values are unlikely in this technology's implementation. A Monte Carlo analysis was performed to understand the distribution of estimated LCAPs based on possible variations in each of the cost components. All components were presumed to have a lifespan (t) between 5 and 15 years, paired with an annual discount rate (r) between 2% and 6%. Calculations were made per kilogram of ADN produced. Details on the TEA methodology are presented in the supplemental information.

The estimated distribution of LCAPs as a function of FE and yield toward ADN is shown in Figure 8. The median ADN cost decreases from US$31.4/kg to $9.4/kg when FE and yield increase from the values obtained in this study to 100%, highlighting the importance of improving the selectivity of the electrochemical transformation. An analysis of the median production cost by individual factors, shown in Table 1, shows that the cost of raw materials (GA) dominates the LCAP, accounting for more than 94% of the estimated cost. This high cost is a consequence of the atom efficiency of the reaction, where 1 kg of ADN

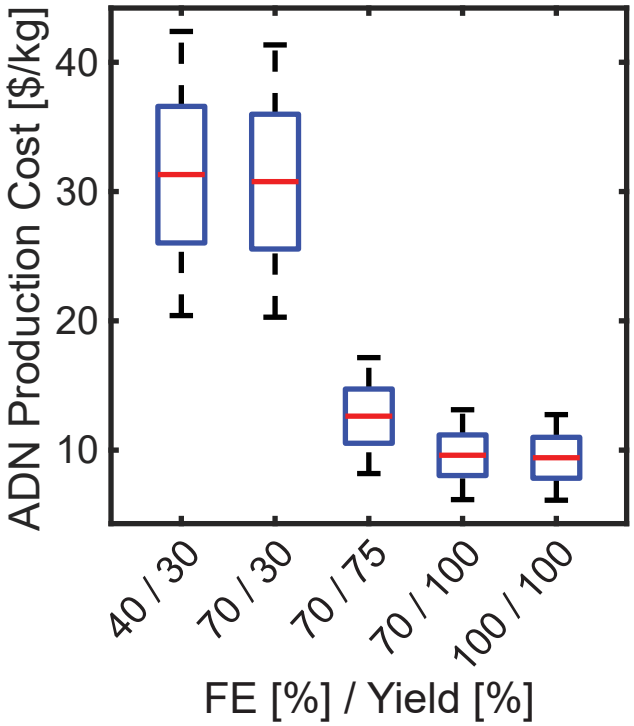

Figure 8. Assessing the economic viability of glutamic acid-derived ADN

Techno-economic assessment of the production cost of adiponitrile (ADN) per kilogram as a function of the reaction selectivity represented by faradic efficiency (FE) and yield. The red line represents the median of the estimated levelized cost of adiponitrile production, the blue box covers the range of prices spanning from the first (25%) to the third (75%) quartile, while the dashed lines span values that are within 1.5 times the interquartile range of the edge of the box.

produced requires at a minimum 2.72 kg of GA (a result of the four by-product CO_2 molecules for each ADN molecule). The high cost of raw materials will likely hinder the economic competitiveness of GA-derived ADN against its petrochemically derived counterpart, whose price currently stands at ~$4.0/kg (based on 2022 market prices).[58] To achieve economic competitiveness, the combined cost of raw GA and its decarboxylation to CPA would have to be below $1.5 per kg of GA, assuming negligible costs for other cost components. Our findings highlight the need to identify cost-competitive sources of GA for the economic viability of the studied ADN process. While biomass-derived ADN may find applications in niche segments of the market able to afford a green premium on the price of chemicals, its deployment at scale will be severely constrained under market conditions where sustainability improvements are not captured on the economic value of products.

Another important insight from this TEA assessment is the interplay between FE and yield. Since the cost of raw material is the determining factor in ADN production, the yield emerges as the target metric to be optimized. In this study, we demonstrated improvements in FE toward ADN through the optimization of electrolyte formulation and operating conditions, which have a positive impact on the reaction yield. In addition, aiming to optimize the FE reduces the parasitic solvent (MeOH) reactions—shown to be prominent in this study—which contributes to additional costs not accounted for in our base estimates. Future studies should aim to identify optimal correlation between FE and yield to enhance the cost-competitiveness of Kolbe reactions. Once key selectivity metrics are further optimized, scale-up of the

Table 1. Cost component breakdown (percentage) of the estimated median production cost of ADN as a function of faradic efficiency and yield

	FE (%)/yield (%)				
	40/30	70/30	70/75	70/100	100/100
Substrate (GA) (%)	96.6	98.3	95.8	94.5	96.5
Capital expense (%)	0.6	0.3	0.7	0.9	0.6
Electricity (%)	2.8	1.4	3.5	4.6	2.9

process will demand a more detailed techno-economic assessment that includes energy considerations, reactor design at larger scale, and separation costs.

Conclusions

The study presented in this article offers new insights into the effect of electrode selection, current density, substrate concentration, supporting ions, pH, and solvent composition on the selectivity and production rate of ADN from biomass-derived CPA. By implementing a hierarchical research approach, HTP reactors allowed us to comprehensively map the parameter space for the electrochemical conversion of CPA to ADN and to rapidly explore relationships between electrolyte composition, electrochemical conditions, and performance metrics. Using these relationships, we investigated the impact of each of the selectivity-driving parameters on reaction performance and then implemented a detailed characterization approach of the reactions under optimal conditions to gain fundamental insights into competing factors that dictate product selectivity.

Our research revealed that Pt electrodes favored the formation of ADN and that its selectivity monotonically increased with increasing current density, reaching a maximum value of ~40% FE at current densities above 275 mA cm^{-2}. We demonstrated that increasing CPA concentrations promote the formation of ADN and that concentrations between 0.7 and 1.0 M are sufficient to achieve high ADN selectivity. We also found that maintaining a high CPA concentration at the electrode surface could impede solvent reactions and enhance the relative probability of PN· radical coupling vs. undergoing oxidation to PN^+. Furthermore, larger alkali cations such as K^+ and Cs^+ favor the formation of ADN, as they can likely limit the availability of water molecules in the electrical double layer and suppress OER.[46] Our study further highlights the importance of pH control and the use of effective buffers to maintain a near-neutral pH, where MeOH oxidation and OER are less prevalent, thereby promoting CPA reactions over solvent reactions. Lastly, our research revealed that ADN production is favored when pure MeOH solvent is used. As the water fraction in the solvent increases, the rate of ADN formation decreases, and completely ceases when pure water solvent is used due to the enhanced OER rates. When using C electrodes, we observed an increased AN production rate, reaching a maximum FE of 35% with a MeOH-water mixture solvent. However, similar to the case of Pt electrodes, when using pure water solvent, water molecules displace CPA-derived intermediates at the electrode interface, resulting in a notable decline in the rate of CPA oxidation.

The experimental insights gained in this study were used to inform a TEA to understand economic viability of ADN production from CPA and to guide future research into technical approaches to impact cost drivers. The TEA estimated the LCAP by considering the cost of electricity, capital expenses, and CPA's raw material cost. Our results demonstrated that the LCAP is expected to be in the range of $10–30/kg, with the cost of raw materials being the predominant cost driver. These results suggest that economic viability of sustainable ADN relies on a combination of technical advances

to enhance the selectivity and energy efficiency of the reaction on sourcing low-cost GA and on the implementation of economic incentives, such as policies that constrain environmental pollution and promote sustainability in chemical manufacture.

Our investigation provides guidelines for the design of electrolytes and optimal electrochemical conditions for CPA electrolysis. While our study used Kolbe electrolysis of CPA as a target reaction, the limitations and strategies highlighted herein are applicable to a wide range of electrochemical decarboxylation reactions. In addition, the hierarchical research approach presented could be used for the accelerated development of sustainable electrochemical processes.

EXPERIMENTAL PROCEDURES

Resource availability

Lead contact

Further information and requests for resources should be directed to and will be fulfilled by the lead contact, Miguel A. Modestino (modestino@nyu.edu).

Materials availability

This study did not generate new materials.

Data and code availability

Any additional information required to reanalyze the data reported in this paper is available from the lead contact upon request.

Materials and chemicals

CPA (95%) was bought from Ambeed (Arlington Heights, IL). Lithium hydroxide, sodium hydroxide, potassium hydroxide, cesium hydroxide hydrate, methanol, adiponitrile (99%), propionitrile (99%), acrylonitrile, sodium formate, and sulfuric acid (95%–97%) were purchased from Sigma-Aldrich. A standard gas hydrocarbon mixture containing 1% CO_2 (99.999%) in nitrogen (99.999%) was purchased from Advanced Specialty Gases (Reno, NV) for gas chromatography calibration.

Two concentrated stock solutions of CPA in methanol and water were prepared close to the point of saturation (in the range of 1.5–2 M for both solvents). An alkali hydroxide was added to the solution up to the desired pH (potassium hydroxide and pH of 7 for all studies except for the experiments on the effect of alkali cation size and effect of pH) measured with a B30PCI pH meter from VWR (Radnor, PA). The stock solutions were then analyzed via ^{1}H nuclear magnetic resonance (NMR) for an accurate quantification of the substrate. For all the reactions carried, a fresh electrolyte solution was prepared by adding the concentrated stock CPA solution to the reactor, diluted to the desired concentration of the substrate and with the desired solvent fraction. The alkali cation is expected to carry the majority of current during reaction.

For detailed reaction characterization experiments, the catholyte consisted of a 1 M solution of sulfuric acid. Nafion 117 purchased from the Fuel Cell Store (College Station, TX) was used to separate the cathodic and anodic chambers. All electrodes used were purchased from Analytical Sales and Services (Flanders, NJ); platinum and graphite rods with 1.6-mm diameter and 31.2-mm length. The platinum rods served as the cathode in all experiments.

Electrochemical characterization

HTP experiments were carried in a 24-well reactor for parallel screening of electrochemically relevant parameters (HTeChem) purchased from Analytical Sales and

Services. Electrolyte preparation for HTP experiments was achieved using Opentrons OT-II pipetting robot (Opentrons, Long Island City, NY). Reactions were performed using a constant current, calibrated DC power supply, 4-output multi-range, 420 W combined output, and vigorous stirring (3,000 rpm). Chronopotentiometry (CP) experiments were carried out by setting the desired current, and the time duration was set as to maintain the total charge transferred constant (500 mA min) along the different current densities evaluated (see Figure S8). Low conversion of the substrate was chosen to maintain a relatively constant concentration of species throughout the reaction and to avoid substantial changes in the bulk pH. A constant electrolyte volume of 0.6 mL was used, and the electrode surface area was 0.72 cm^2 Figures S9 and S10 show sweep voltammetry and electrochemical impedance spectroscopy (EIS) data for relevant reaction conditions performed in the HTP experiments.

Detailed reaction characterization experiments were performed in an H cell fabricated using a Stratasys Objet30 3D printer, with VeroClear resin as printing material (Figure S4). The cathode and anode sides were separated by a Nafion 117 membrane. The anode side was sealed to the atmosphere and equipped with a nitrogen purge to aid in the collection of gas products. Nitrogen was flowed at a rate of 9.2 sccm into the reactor. A cold trap was incorporated downstream of the nitrogen and gas products to condense any evaporated products. Gas products were collected using a Tedlar sample bag. Viton O-rings were used to seal the membrane between the two chambers, and a Ag/AgCl electrode in saturated KCl solution was used as reference electrode. EIS and CP experiments were performed using a BioLogic VSP-300 potentiostat equipped with a $\pm$1 A/$\pm$48 V booster. A constant electrolyte volume of 1.5 mL was used, and the working electrode surface area was 0.50 cm^2. Electrolyte was vigorously stirred with 2 × 2 mm micro stir bars.

Chemical analysis

HTP liquid products were analyzed by ^{1}H NMR using a Spinsolve 60 NMR spectrometer (Magritek, Aachen, Germany), with a delay time of 30 s, 32 scans per measurement, and without solvent suppression. The samples consisted of 75% electrolyte and 25% of a standard 0.25 M solution of sodium formate for product quantification. See Figures S11 and S12 for sample spectra.

Detailed reaction characterization liquid products were analyzed via ^{1}H NMR using a Bruker Avance III 400 NMR spectrometer, with a delay time of 8 s, 16 scans per measurement, and without solvent suppression. The samples consisted of 60% anolyte, 10% of a standard 0.25 M solution of sodium formate for product quantification, and 30% DMSO-d6. See Figure S13 for sample spectra. Gas products were identified and quantified by gas chromatography using an Agilent 990 Micro GC equipped with a MolSieve 5A column (channel 1) and a PoraPLOT Q column (channel 2) (Agilent, Santa Clara, CA). Acquisition parameters for channel 1 were: injection temperature 110°C, injection time 80 ms, column temperature 80°C, carrier gas He, and run time 300 s. Acquisition parameters for channel 2 were injection temperature 110°C, injection time 200 ms, column temperature 70°C, carrier gas He, and run time 300 s. A standard gas mixture containing CO_2 was used as a reference.

SUPPLEMENTAL INFORMATION

Supplemental information can be found online at https://doi.org/10.1016/j.checat.2024.100998.

ACKNOWLEDGMENTS

We thank the New York University (NYU) Tandon School of Engineering and the National Science Foundation for their generous financial support. This material is based upon work supported by the National Science Foundation under grant no. 1943972. The authors acknowledge the NYU Tandon Makerspace for device fabrication support.

AUTHOR CONTRIBUTIONS

Conceptualization, R.M. and M.A.M.; methodology, R.M., C.K.B., A.L.C., and M.A.M.; software, R.M.; formal analysis, R.M.; investigation, R.M., E.R., and M.K.P.; writing – original draft, R.M.; writing – review & editing, C.K.B. and M.A.M.; visualization, R.M.; supervision, M.A.M.; project administration, M.A.M.; funding acquisition, M.A.M.

DECLARATION OF INTERESTS

M.A.M. is a co-founder of and has a financial interest in Sunthetics, Inc., a start-up company in the machine-learning optimization space.

DECLARATION OF GENERATIVE AI AND AI-ASSISTED TECHNOLOGIES IN THE WRITING PROCESS

During the preparation of this work the authors used OpenAI's ChatGPT in order to improve language and readability. After using this tool/service, the authors reviewed and edited the content as needed and take full responsibility for the content of the publication.

Received: January 18, 2024
Revised: March 14, 2024
Accepted: April 16, 2024
Published: May 8, 2024

REFERENCES

1. Lucas, F.W.S., Grim, R.G., Tacey, S.A., Downes, C.A., Hasse, J., Roman, A.M., Farberow, C.A., Schaidle, J.A., and Holewinski, A. (2021). Electrochemical Routes for the Valorization of Biomass-Derived Feedstocks: From Chemistry to Application. ACS Energy Lett. 1205–1270. https://doi.org/10.1021/acsenergylett.0c02692.

2. Shanks, B.H., and Keeling, P.L. (2017). Bioprivileged molecules: creating value from biomass. Green Chem. *19*, 3177–3185. https://doi.org/10.1039/c7gc00296c.

3. Holzhäuser, F.J., Mensah, J.B., and Palkovits, R. (2020). (Non-)Kolbe electrolysis in biomass valorization – a discussion of potential applications. Green Chem. *22*, 286–301. https://doi.org/10.1039/c9gc03264a.

4. Mathison, R., Ramos Figueroa, A.L., Bloomquist, C., and Modestino, M.A. (2023). Electrochemical Manufacturing Routes for Organic Chemical Commodities. Annu. Rev. Chem. Biomol. Eng. *14*, 85–108. https://doi.org/10.1146/annurev-chembioeng-101121-090840.

5. Palkovits, S., and Palkovits, R. (2019). The Role of Electrochemistry in Future Dynamic Bio-Refineries: A Focus on (Non-)Kolbe Electrolysis. Chem. Ing. Tech. *91*, 699–706. https://doi.org/10.1002/cite.201800205.

6. Iglesias, J., Martínez-Salazar, I., Maireles-Torres, P., Martin Alonso, D., Mariscal, R., and López Granados, M. (2020). Advances in catalytic routes for the production of carboxylic acids from biomass: a step forward for sustainable polymers. Chem. Soc. Rev. *49*, 0306-0012. https://doi.org/10.1039/d0cs00177e.

7. Cho, E.J., Trinh, L.T.P., Song, Y., Lee, Y.G., and Bae, H.J. (2020). Bioconversion of biomass waste into high value chemicals. Bioresour. Technol. *298*, 122386. https://doi.org/10.1016/j.biortech.2019.122386.

8. Mariscal, R., Maireles-Torres, P., Ojeda, M., Sádaba, I., and López Granados, M. (2016). Furfural: a renewable and versatile platform molecule for the synthesis of chemicals and fuels. Energy Environ. Sci. *9*, 1144–1189. https://doi.org/10.1039/c5ee02666k.

9. Garedew, M., Lin, F., Song, B., DeWinter, T.M., Jackson, J.E., Saffron, C.M., Lam, C.H., and Anastas, P.T. (2020). Greener Routes to Biomass Waste Valorization: Lignin Transformation Through Electrocatalysis for Renewable Chemicals and Fuels Production. ChemSusChem *13*, 4214–4237. https://doi.org/10.1002/cssc.202000987.

10. Du, X., Zhang, H., Sullivan, K.P., Gogoi, P., and Deng, Y. (2020). Electrochemical Lignin Conversion. ChemSusChem *13*, 4318–4343. https://doi.org/10.1002/cssc.202001187.

11. Angulo, A., Elizarraras, C., Shin, J.H., van Riel, A., Akashige, T., and Modestino, M. (2023). Understanding the electrocatalytic oxidation of propionic acid for the sustainable production of ethylene. RSC Sustain. *1*, 2270–2276.. https://doi.org/10.1039/d3su00347g.

12. Hayes, G., Laurel, M., MacKinnon, D., Zhao, T., Houck, H.A., and Becer, C.R. (2023). Polymers without Petrochemicals: Sustainable Routes to Conventional Monomers. Chem. Rev. *123*, 2609–2734. https://doi.org/10.1021/acs.chemrev.2c00354.

13. Tolman, C., McKinney, R., Seidel, W., Druliner, J., and Stevens, W. (1985). Homogeneous nickel-catalyzed olefin hydrocyanation. In Advances in Catalysis (Elsevier), pp. 1–46.

14. Tolman, C.A. (1986). Steric and electronic effects in olefin hydrocyanation at Du Pont: A scientific and industrial success story. J. Chem. Educ. *63*, 199.

15. Shu, X., Jiang, Y.-Y., Kang, L., and Yang, L. (2020). Ni-Catalyzed hydrocyanation of alkenes with formamide as the cyano source. Green Chem. *22*, 2734–2738.

16. Baizer, M.M. (1964). Electrolytic Reductive Coupling: I. Acrylonitrile. J. Electrochem. Soc. *111*, 215.

17. Blanco, D.E., Dookhith, A.Z., and Modestino, M.A. (2019). Enhancing selectivity and efficiency in the electrochemical synthesis of adiponitrile. React. Chem. Eng. *4*, 8–16. https://doi.org/10.1039/c8re00262b.

18. Blanco, D.E., Lee, B., and Modestino, M.A. (2019). Optimizing organic electrosynthesis through controlled voltage dosing and artificial intelligence. Proc. Natl. Acad. Sci. USA *116*, 17683–17689. https://doi.org/10.1073/pnas.1909985116.

19. Botte, G.G. (2014). Electrochemical Manufacturing in the Chemical Industry. Electrochem. Soc. Interface *23*, 49–55. https://doi.org/10.1149/2.F04143if.

20. Scott, E., Peter, F., and Sanders, J. (2007). Biomass in the manufacture of industrial products—the use of proteins and amino acids. Appl. Microbiol. Biotechnol. *75*, 751–762.

21. Lammens, T.M., Franssen, M.C.R., Scott, E.L., and Sanders, J.P.M. (2012). Availability of protein-derived amino acids as feedstock for the production of bio-based chemicals. Biomass Bioenergy *44*, 168–181. https://doi.org/10.1016/j.biombioe.2012.04.021.

22. Tuck, C.O., Pérez, E., Horváth, I.T., Sheldon, R.A., and Poliakoff, M. (2012). Valorization of biomass: deriving more value from waste. Science *337*, 695–699.

23. Dai, J.J., Huang, Y.B., Fang, C., Guo, Q.X., and Fu, Y. (2012). Electrochemical synthesis of adiponitrile from the renewable raw material glutamic acid. ChemSusChem *5*, 617–620. https://doi.org/10.1002/cssc.201100776.

24. Lammens, T.M., Le Nôtre, J., Franssen, M.C.R., Scott, E.L., and Sanders, J.P.M. (2011). Synthesis of biobased succinonitrile from glutamic acid and glutamine. ChemSusChem *4*, 785–791. https://doi.org/10.1002/cssc.201100030.

25. Le Nôtre, J., Scott, E.L., Franssen, M.C.R., and Sanders, J.P.M. (2011). Biobased synthesis of acrylonitrile from glutamic acid. Green Chem. *13*, 807–809. https://doi.org/10.1039/c0gc00805b.

26. Xu, X., But, A., Wever, R., and Hollmann, F. (2020). Towards Preparative Chemoenzymatic Oxidative Decarboxylation of Glutamic Acid. ChemCatChem *12*, 2180–2183. https://doi.org/10.1002/cctc.201902194.

27. Kümper, J., Meyers, J., Sebers, R., Kurig, N., and Palkovits, R. (2023). Electrochemical transformation of d,l-glutamic acid into acrylonitrile. Green Chem. *25*, 6231–6237. https://doi.org/10.1039/d3gc01045g.

28. Kolbe, H. (1849). Untersuchungen über die Elektrolyse organischer Verbindungen. Justus Liebigs Ann. Chem. *69*, 257–294.

29. Vijh, A.K., and Conway, B.E. (1967). Electrode kinetic aspects of the Kolbe reaction. Chem. Rev. *67*, 623–664.

30. Andreev, V.N., Grinberg, V.A., Dedov, A.G., Loktev, A.S., Moiseev, I.I., and Tsivadze, A.Y. (2013). Electrocatalytic biomass conversion into petrochemicals. Review. Prot. Met. Phys. Chem. Surf. *49*, 32–39. https://doi.org/10.1134/s2070205113010024.

31. Wiebe, A., Gieshoff, T., Möhle, S., Rodrigo, E., Zirbes, M., and Waldvogel, S.R. (2018). Electrifying Organic Synthesis. Angew. Chem. Int. Ed. Engl. *57*, 5594–5619. https://doi.org/10.1002/anie.201711060.

32. Qiu, Y., Lopez-Ruiz, J.A., Zhu, G., Engelhard, M.H., Gutiérrez, O.Y., and Holladay, J.D. (2022). Electrocatalytic decarboxylation of carboxylic acids over RuO2 and Pt nanoparticles. Appl. Catal. B Environ. *305*, 121060. https://doi.org/10.1016/j.apcatb.2021.121060.

33. Rein, J., Annand, J.R., Wismer, M.K., Fu, J., Siu, J.C., Klapars, A., Strotman, N.A., Kalyani, D., Lehnherr, D., and Lin, S. (2021). Unlocking the Potential of High-Throughput Experimentation for Electrochemistry with a Standardized Microscale Reactor. ACS Cent. Sci. *7*, 1347–1355. https://doi.org/10.1021/acscentsci.1c00328.

34. Boeke, J.D., Laurent, J., Martin, A., and Mita, P. (2023). Methods and Compositions for Rapid and High Throughput Diagnosis. US patent US11667962B2. filed September 17, 2021, and granted June 6, 2023.

35. Frey, D., Neyerlin, K.C., and Modestino, M.A. (2023). Bayesian optimization of electrochemical devices for electrons-to-molecules conversions: the case of pulsed CO2 electroreduction. React. Chem. Eng. *8*, 323–331. https://doi.org/10.1039/d2re00285j.

36. Bloomquist, C.K., Dogan, M., Harris, J.S., Herzog, B.D., Tenn III, W.J., Aydil, E.S., and Modestino, M.A. (2024). Understanding the effects of forced and bubble-induced convection in transport-limited organic electrosynthesis. React. Chem. Eng. *9*, 930–939. https://doi.org/10.1039/d3re00579h.

37. Schäfer, H.-J. (1990). Recent contributions of kolbe electrolysis to organic synthesis. In Electrochemistry IV, *152*, E. Steckhan, ed. Topics in Current Chemistry. (Springer), pp. 91–151.

38. Levy, P., Sanderson, J., Kispert, R., and Wise, D. (1981). Biorefining of biomass to liquid fuels and organic chemicals. Enzym. Microb. Technol. *3*, 207–215.

39. Liu, S., Govindarajan, N., Prats, H., and Chan, K. (2022). Understanding the reaction mechanism of Kolbe electrolysis on Pt anodes. Chem Catal. *2*, 1100–1113. https://doi.org/10.1016/j.checat.2022.02.014.

40. Dickinson, T., and Wynne-Jones, W.F.K. (1962). Mechanism of Kolbe's electrosynthesis. Part 1.—Anode potential phenomena. Trans. Faraday Soc. *58*, 382–387.

41. Yuan, G., Wu, C., Zeng, G., Niu, X., Shen, G., Wang, L., Zhang, X., Luque, R., and Wang, Q. (2019). Kolbe Electrolysis of Biomass-Derived Fatty Acids Over Pt Nanocrystals in an Electrochemical Cell. ChemCatChem *12*, 642–648. https://doi.org/10.1002/cctc.201901443.

42. Coleman, J.P., Lines, R., Utley, J.H.P., and Weedon, B.C.L. (1974). Electro-organic reactions. Part II. Mechanism of the kolbe electrolysis of substituted phenylacetate ions. J. Chem. Soc. Perkin Trans. II, 1064–1069.

43. Qiu, Y., Lopez-Ruiz, J.A., Sanyal, U., Andrews, E., Gutiérrez, O.Y., and Holladay, J.D. (2020). Anodic electrocatalytic conversion of carboxylic acids on thin films of RuO2, IrO2, and Pt. Appl. Catal. B Environ. *277*, 119277. https://doi.org/10.1016/j.apcatb.2020.119277.

44. Nilges, P., dos Santos, T.R., Harnisch, F., and Schröder, U. (2012). Electrochemistry for biofuel generation: Electrochemical conversion of levulinic acid to octane. Energy Environ. Sci. *5*, 5231–5235. https://doi.org/10.1039/c1ee02685b.

45. Stang, C., and Harnisch, F. (2016). The Dilemma of Supporting Electrolytes for Electroorganic Synthesis: A Case Study on Kolbe Electrolysis. ChemSusChem *9*, 50–60. https://doi.org/10.1002/cssc.201501407.

46. Blanco, D.E., Atwi, R., Sethuraman, S., Lasri, A., Morales, J., Rajput, N.N., and Modestino, M.A. (2020). Effect of Electrolyte Cations on Organic Electrosynthesis: The Case of Adiponitrile Electrochemical Production. J. Electrochem. Soc. *167*, 155526. https://doi.org/10.1149/1945-7111/abc766.

47. Resasco, J., Chen, L.D., Clark, E., Tsai, C., Hahn, C., Jaramillo, T.F., Chan, K., and Bell, A.T. (2017). Promoter effects of alkali metal cations on the electrochemical reduction of carbon dioxide. J. Am. Chem. Soc. *139*, 11277–11287.

48. Klocke, E., Matzeit, A., Gockeln, M., and Schäfer, H.J. (1993). Electroorganic Synthesis, 55[1]. Influences on the Selectivity of the Kolbe versus the Non-Kolbe Electrolysis in the Anodic Decarboxylation of Carboxylic Acids. Chem. Ber. *126*, 1623–1630.

49. Nordkamp, M.O., Mei, B., Venderbosch, R., and Mul, G. (2022). Study on the Effect of Electrolyte pH during Kolbe Electrolysis of Acetic Acid on Pt Anodes. ChemCatChem *14*. https://doi.org/10.1002/cctc.202200438.

50. Melle, G.B., Hartl, F.W., Varela, H., and Sitta, E. (2018). The effect of solution pH on the oscillatory electro-oxidation of methanol. J. Electroanal. Chem. *826*, 164–169. https://doi.org/10.1016/j.jelechem.2018.08.033.

51. Fornaciari, J.C., Weng, L.-C., Alia, S.M., Zhan, C., Pham, T.A., Bell, A.T., Ogitsu, T., Danilovic, N., and Weber, A.Z. (2022). Mechanistic understanding of pH effects on the oxygen evolution reaction. Electrochim. Acta *405*, 139810. https://doi.org/10.1016/j.electacta.2021.139810.

52. Harnisch, F., and Schröder, U. (2019). Tapping Renewables: A New Dawn for Organic Electrosynthesis in Aqueous Reaction Media. Chemelectrochem *6*, 4126–4133. https://doi.org/10.1002/celc.201900456.

53. Rodriguez, C.A., Modestino, M.A., Psaltis, D., and Moser, C. (2014). Design and cost considerations for practical solar-hydrogen generators. Energy Environ. Sci. *7*, 3828–3835. https://doi.org/10.1039/c4ee01453g.

54. IEA (2023). Electricity Market Report 2023. https://www.iea.org/reports/electricity-market-report-2023.

56. James, B.D., Huya-Kouadio, J.M., Houchins, C., and DeSantis, D.A. (2018). Mass production cost estimation of direct H_2 PEM fuel cell systems for transportation applications: 2018 Update. Strategic Analysis Inc. https://www.energy.gov/eere/fuelcells/articles/mass-production-cost-estimation-direct-h2-pem-fuel-cell-systems-7.

56. IndexBox (2023). World - Glutamic Acid and its Salts - Market Analysis, Forecast, Size, Trends and Insights. https://www.indexbox.io/search/glutamic-acid-market/.

57. Lammens, T.M., Gangarapu, S., Franssen, M.C., Scott, E.L., and Sanders, J.P. (2012). Techno-economic assessment of the production of bio-based chemicals from glutamic acid. Biofuel. Bioprod. Biorefin. 6, 177–187. https://doi.org/10.1002/bbb.349.

58. Grand View Research (2022). Adiponitrile Market Size, Share & Trends Analysis Report by Application (Nylon Synthesis, HDI), by End-Use (Automobile, Chemical Intermediate), by Region, and Segment Forecasts, 2023–2030. https://www.grandviewresearch.com/industry-analysis/adiponitrile-market.